

September 1985

LRP 269/85

**COMPUTATIONAL MODELS FOR WAVE-PARTICLE
INTERACTIONS**

S. Succi, K. Appert, W. Core, H. Hamnén,
T. Hellsten and J. Vaclavik

Paper presented at the

**3rd European Workshop on Problems in the Numerical Modeling of Plasmas
NUMOP 85**

Varenna, Italy, 10 - 13 September 1985

COMPUTATIONAL MODELS FOR WAVE-PARTICLE INTERACTIONS

S. Succi, K. Appert, W. Core*, H. Hamnén*, T. Hellsten*
and J. Vaclavik

Centre de Recherches en Physique des Plasmas
Association EURATOM - Confédération Suisse
Ecole Polytechnique Fédérale de Lausanne
21, Av. des Bains, CH-1007 Lausanne, Switzerland

* JET Joint Undertaking, Abingdon, OX14 3EA, Great Britain

ABSTRACT

A 2-D finite-element evolution Fokker-Planck code, BACCHUS, is presented. The originally current-drive version and a more recent bounce-averaged version are discussed in some detail. A $1\frac{1}{2}$ -D quasi-linear code, RUNAWAY, is also described, especially to elucidate the major difficulties arising when the wave-particle interaction is included in a self-consistent way. Finally, some very preliminary information concerning a new 2-D quasi-linear code, presently under development at CRPP, is given.

1. INTRODUCTION

A good comprehension of the physics of wave-particle interactions is essential for the interpretation of the present-day rf-heating and current-drive experiments. It is therefore important to develop accurate numerical models which retain as much physics as possible and have at the same time an acceptable degree of efficiency. In this respect, a basic distinction can be made between models which follow the simultaneous evolution of the particle distribution function and the wave spectral distribution (henceforth referred to as "quasi-linear" models), and those in which only the particle distribution function is computed ("Fokker-Planck" models). While for the latter a certain number of standard techniques is available (linear PDE solvers), for the former no well-established tools seem to have been devised as yet. Moreover, while for 2-D Fokker-Planck models the computing power presently available already makes possible the treatment of spatially inhomogeneous plasmas [1], in the quasi-linear models such an extension still appears problematic.

This paper is mainly concerned with the description of a 2-D finite-element Fokker-Planck code, BACCHUS, originally developed for Lower Hybrid Range of Frequency (LHRF) purposes and recently adapted for Ion Cyclotron Range of Frequency (ICRF) studies. A $1\frac{1}{2}$ -D quasi-linear code, RUNAWAY, is also described, especially to elucidate the major difficulties one meets when the wave-particle interaction is included in a self-consistent way. Profiting from the experience gained from BACCHUS and RUNAWAY, one can hope to overcome these difficulties.

The effort made in this direction will lead to a new 2-D quasi-linear code presently under development at CRPP.

2. BACCHUS; A 2-D FINITE-ELEMENT FOKKER-PLANCK CODE

2.1 The Physical Model

BACCHUS is a code designed to solve the following initial value problem:

$$\partial f / \partial t = \left(\delta f / \delta t \right)_{\text{COLL}} + \left(\delta f / \delta t \right)_{\text{IND-E}} + \left(\delta f / \delta t \right)_{\text{WAVES}}, \quad (1a)$$

$$f(\vec{v}, 0) = (2\pi)^{-3/2} \exp(-v^2/2), \quad (1b)$$

where $f(\vec{v}, t)$ represents the test particle distribution function in the velocity space. Cylindrical coordinates, v_{\parallel} , v_{\perp} are adopted. In eq. (1) we utilise the following normalization $v \rightarrow vv_{te}$, $t \rightarrow tv_{ee}^{-1}$, $f \rightarrow fnv_{te}^3$, $E \rightarrow EE_D$, where $E_D = mv_{te}v_{ee}/2e$ is the Dreicer field and $v_{ee} = \omega_{pe}^4 \cdot \ln\Lambda / 4\pi nv_{te}^3$ is the electron-electron collision frequency. In the r.h.s. of eq. (1a), $(\delta f / \delta t)_{\text{COLL}}$ is a collision operator describing the interaction between the evolving test particle distribution function and a background of electrons and ions of constant temperature. This background acts as a sink of the energy and momentum gained by the test particles. Since we are mainly

interested in the evolution of the fast electrons, $v \gg v_{te}$, the collision operator is linearized about a Maxwellian. In addition to the linearization, a minor modification is required to avoid negative eigenvalues for $v < v_{te}$ (they arise because the linearization utilizes the hypotheses $v \gg v_{te}$). The resulting collision operator is a fair approximation even for $v \sim v_{te}$. Because of its simplicity we use it wherever possible. In the application of BACCHUS to minority ions, however, it is replaced by a bounce-averaged operator including the Rosenbluth potentials. This will be described in Section 4.

For the LHRF case, the operator reads :

$$(\delta f / \delta t)_{\text{coll.}} = \vec{\nabla} \cdot [(\vec{R}_c + \vec{D}_c \cdot \vec{\nabla}) f] , \quad (2)$$

where $\vec{R}_c = \vec{v} / v^3$, (3)

$$\vec{D}_c = \frac{1}{2} \left[\left(\frac{2}{v^2} - (1+Z) \right) \frac{\vec{v} \vec{v}}{v^3} + \left(\frac{1+Z}{v} \right) \vec{I} \right]$$

and Z denotes the ion charge state.

The term $(\delta f / \delta t)_{\text{IND-E}}$ describes the effect of the inductive field

$$(\delta f / \delta t)_{\text{IND.E}} = \vec{E} \cdot \vec{\nabla} f , \quad (4)$$

where evidently $\vec{E} = E \hat{e}_{\parallel}$.

Finally, the term $(\delta f / \delta t)_{\text{WAVES}}$ represents the effect of the energy deposition of lower-hybrid and/or electron-cyclotron waves, resulting

from the Cerenkov and the first Doppler resonance respectively. Both are modelled by diffusion operators:

$$(\delta f / \delta t)_{LH} = \frac{\partial}{\partial v_{\parallel}} \left[\frac{D_{LH}}{|v_{\parallel}|^3} \frac{\partial}{\partial v_{\parallel}} \right] f, \quad (5)$$

$$(\delta f / \delta t)_{EC} = \frac{1}{v_{\perp}} \frac{\partial}{\partial v_{\perp}} \left[\frac{v_{\perp}}{v_{\parallel}} D_{EC} \frac{\partial}{\partial v_{\perp}} \right] f. \quad (6)$$

The whole problem (1) can thus be reformulated in terms of a linear diffusion-advection PDE:

$$\partial f / \partial t = \vec{\nabla} \cdot (\vec{R} f + \vec{D} \cdot \vec{\nabla} f), \quad (7)$$

where

$$\begin{aligned} \vec{R} &= \vec{R}_c + \vec{E}, \\ \vec{D} &= \vec{D}_c + \vec{D}_{LH} + \vec{D}_{EC}. \end{aligned}$$

3. THE NUMERICAL TREATMENT

The problem represented by eq. (7) is solved by the finite element method [2]. Following the main lines of this method, we reformulate the problem in the weak (Galerkin) form:

$$\langle g, \frac{\partial f}{\partial t} - \vec{\nabla} \cdot (\vec{R} f + \vec{D} \cdot \vec{\nabla} f) \rangle = 0, \quad (8)$$

where g is any test function in a suitable functional space, G , which possesses a scalar product $\langle g, h \rangle = \iint_{\mathcal{D}} g(v_{\parallel}, v_{\perp}) h(v_{\parallel}, v_{\perp}) d_2 v$, where

$d_2v = v_1 dv_{\parallel} dv_{\perp}$ and \mathcal{D} is the unbounded domain $\mathcal{D} = \{v_{\parallel}, v_{\perp} \mid -\infty < v_{\parallel} < \infty, v_{\perp} \geq 0\}$

After integration by parts, eq. (8) becomes

$$\iint_{\mathcal{D}} \left[g \left(\frac{\partial f}{\partial t} - \vec{E} \cdot \vec{\nabla} f \right) + \vec{\nabla} g \cdot \left(\vec{R}_c f + \vec{D} \cdot \vec{\nabla} f \right) \right] d_2v = \int_{\partial \mathcal{D}} g \left(\vec{R}_c f + \vec{D} \cdot \vec{\nabla} f \right) \cdot d\vec{v}_s \quad (9)$$

where $d\vec{v}_s$ represents the directed line element of the boundary $\partial \mathcal{D}$ of the domain \mathcal{D} . Since only first order derivatives are involved in eq. (9), the most convenient choice for G is the Sobolev space $H^1(\mathcal{D}) \times H^1(\mathcal{D})$.

3.1 Finite Velocity Domain

We search for an approximate solution of eq. (9) for g and f lying in a finite-dimensional subspace S^N of $H^1(\mathcal{D}) \times H^1(\mathcal{D})$. Since we use finite elements, we first need to reduce the unbounded domain to a corresponding bounded one, Δ ,

$$\Delta = \left\{ v_{\parallel}, v_{\perp} \mid V_1 \leq v_{\parallel} \leq V_2; 0 \leq v_{\perp} \leq V_4 \right\} \quad (10)$$

In order to neglect the boundary term in eq. (9) we assume the natural boundary condition

$$\int_{\partial \mathcal{D}} \left(\vec{R}_c f + \vec{D} \cdot \vec{\nabla} f \right) \cdot d\vec{v}_s = 0 \quad .$$

This poses no problem as long as no steady electric field is present: one just lets V_1, V_2, V_4 be "large" enough. Once the E-field is

included the flux at the boundary is not zero (it is precisely the runaway rate) and the whole problem of finding a steady state solution of eq. (1) has to be reconsidered. We will comment on this point later.

3.2 Discrete Velocities

The velocity space is discretized by introducing the finite dimensional subspace S^N of $H^1(\Delta) \times H^1(\Delta)$. Both the test function g and the approximate solution f^N of eq. (9) are assumed to lie in the same subspace S^N

$$g = \Psi_i^N(v_{11}, v_{12}) , \quad i = 1, N \quad , \quad (11)$$

$$f = \sum_{j=1}^N f_j(t) \Psi_j^N(v_{11}, v_{12}) \quad . \quad (12)$$

Substituting the expressions (11) and (12) into eq. (9) we obtain a system of N ordinary differential equations of first order for the N expansion coefficients $f_j(t)$:

$$\sum_{j=1}^N A_{ij} \dot{f}_j = \sum_{j=1}^N B_{ij} f_j \quad , \quad (13)$$

where

$$A_{ij} = \iint_{\Delta} \Psi_i \Psi_j d_2 v \quad (14)$$

and

$$B_{ij} = \iint_{\Delta} [\Psi_i \vec{E} \cdot \vec{\nabla} \Psi_j - \vec{\nabla} \Psi_i \cdot (\vec{R}_c \Psi_j + \vec{D} \cdot \vec{\nabla} \Psi_j)] d_2 v \quad . \quad (15)$$

We note that the matrix A_{ij} is hermitian and positive definite, whereas the matrix B_{ij} is the sum of hermitian (diffusive) and anti-hermitian (convective) components.

As basis functions we have chosen the bilinear pyramid functions $\hat{e}_i(v_{\parallel}, v_{\perp})$ shown in Fig. 1. They are 0 on the boundary of the support and take the value 1 at the centre. With this choice, each pivot Ψ_i 'interacts' with at most nine Ψ_j 's, so that the matrices A and B are sparse with a block tribanded structure. A non-equidistant mesh is allowed by the accumulation technique described below.

Given the interval $[a,b]$, we introduce an unnormalized, positive definite, density weight function $W(z)$. The sequence of the mesh points $\{z_i; i=1,N\}$, is then obtained by:

$$\int_{z_i}^{z_{i+1}} W(z) dz = W_0/N \quad ,$$

with $z_1=a$ and $z_N=b$ and $W_0 = \int_a^b W(z) dz$. The function W is chosen in the form:

$$W(v_{\parallel}) = C_1 + C_2 v_{\parallel} + C_3 \exp\left[-\frac{1}{2} \left(\frac{v_{\parallel} - C_4}{C_5}\right)^2\right] + C_6 \exp\left[-\frac{1}{2} \left(\frac{v_{\parallel} - C_7}{C_8}\right)^2\right]$$

and the same for the v_{\perp} -axis with the replacement $C_i \rightarrow C_{i+8}$, $i=1,8$. The standard values assumed throughout the paper, henceforth referred to as s.n.u. (standard non-uniform), are:

$$C_1=0.24, C_2=0, C_3=0.4, C_4=2.5, C_5=1, C_6=0.24, C_7=-2.5, C_8=1$$
$$C_9=C_1, C_{10}=C_2, C_{11}=C_3, C_{12}=C_4, C_{13}=C_5, C_{17}=0, C_{15}=1, C_{16}=1$$

The possibility of adopting non-uniform meshes without losing an order of accuracy is one of the basic advantages of the finite element method when compared to the finite difference method. This feature will be discussed in section 5.

3.3 Time Discretization

The system of ordinary differential equations (13) is solved with a two-level scheme on a non-equidistant time lattice: $\{t_n\}$. In matrix notation:

$$A \left(\frac{f_{n+1} - f_n}{t_{n+1} - t_n} \right) = B \left(f_{n+1} \cdot \delta + f_n \cdot (1 - \delta) \right), \quad (16)$$

where δ is a parameter ranging from 0 (explicit) to 1 (fully implicit). This scheme is unconditionally stable and of second order in accuracy if $\delta = 1/2$. Rearranging the terms in eq. (16), we obtain

$$A f_{n+1} = B f_n, \quad (17)$$

with

$$A = A - B \Delta t \delta, \quad B = A + B \Delta t (1 - \delta). \quad (18)$$

The time step is dynamically adapted to the time evolution by an automatic control which prevents relative changes of f larger than a given value, typically 5%.

3.4 The Method of Solution

Equation (17) represents a set of $N = N_x \cdot N_y$ algebraic equations for the N unknowns f_i , $i = 1, N$ ($N_x =$ number of points along v_{\parallel} and N_y along v_{\perp}), which has to be solved at each time step. The unknown array f_i is numerated row by row as indicated in Fig. 2. The solution can be obtained by a direct Gauss elimination method which is exact but requires a large amount of operations and memory space (typically $t_{CPU} \sim NM^2$ and $W_{CPU} \sim NM$, where N is the length of the matrix and M its bandwidth). Given the very sparse nature of the matrices, it is reasonable to consider approximate iterative procedures. Therefore, an iterative method has also been developed which is based on the following scheme: The $(l+1)$ -th iteration is defined by:

$$A_M f_{M,n+1}^{(l+1)} = B f_n^{(l+1)} - A_D f_{D,n+1}^{(l+1)} - A_U f_{U,n+1}^{(l)} \equiv b_{n+1}^{(l+1)}, \quad (19)$$

where D (down), M (middle) and U (up) indicate three successive rows in the y -direction and, as a consequence, the three matrices $A_{D,M,U}$ are tridiagonal of the dimension N_x . The iteration cycle is terminated by the following closure condition:

$$\varepsilon^{(l+1)} = 2 \text{Max}_i \left\{ \frac{|f_i^{(l+1)} - f_i^{(l)}|}{|f_i^{(l+1)}| + |f_i^{(l)}|} \right\} < \varepsilon_c. \quad (20)$$

On adopting this scheme one reduces the 2-D problem of dimension $N_x * N_y$ into N_y 1-D problems of dimension N_x and, above all, one need not store the matrix A in "full" format, i.e., including the zero elements. This is certainly very advantageous from the point of view of central memory occupation and can sometimes prove profitable also from the point of view of c.p.u. time. This holds, of course, only if the scheme (19) converges, which is not guaranteed since the matrix A_M is generally not positive definite (due to the advective terms). However, due to the time step control the symmetric component of A_M dominates and convergence can be expected, at least for values of the electric field satisfying the Courant-Levy-Friedrichs condition: $E < \Delta v_{\parallel} / \Delta t$.

3.5 Diagnostics and Conservation Properties of the Numerical Scheme

It can be shown [3] that due to the identities

$$1 \equiv \sum_{i=1}^N \psi_i \quad , \quad \bar{v} \equiv \sum_{i=1}^N (\bar{v}_i) \psi_i \quad ,$$

the numerical scheme, eq. (13), conserves exactly^(*) the density and the momenta whenever they are physical invariants. However, due to the presence of the steady electric field, which can convect a macroscopic quantity away from any finite region of the velocity space in a finite time (roughly a collision time evaluated at $v = v_c = (E_D/E)^{1/2}$),

(*) Within the accuracy of the quadrature scheme by which the matrix elements are evaluated: in our case a 2x2 gaussian quadrature.

the system represented by eq. (7) does not exhibit any invariant. Moreover, even in the absence of the steady electric field, the only conserved quantity is the particle number since the rf operator and collision operator conserve neither momentum nor energy. This means that we have to resort to other diagnostic tools. They are presented in section 5.

4. FROM THE CURRENT-DRIVE TO AN ICRF CODE

According to the "Olympian" philosophy [4], BACCHUS has been developed following the criterion of high modularity. This means that its structure is fairly independent of the details of the physics which is implemented, so that rapid adaptations are possible with a minor programming effort. In this spirit, BACCHUS has recently been adapted to ICRF purposes, as we shall briefly describe. Our starting point is the local bounce-averaged Fokker-Planck equation [5]:

$$\frac{\partial f}{\partial t} = \frac{1}{\langle \frac{v_{\parallel 0}}{v_{\parallel}} \rangle} \left[\left\langle \frac{N_{H0}}{v_{\parallel}} \left(\frac{\delta f}{\delta t} \right)_{\text{COLL}} \right\rangle + \left\langle \frac{N_{H0}}{v_{\parallel}} \left(\frac{\delta f}{\delta t} \right)_Q \right\rangle + \left\langle \frac{N_{H0}}{v_{\parallel}} S \right\rangle \right], \quad (21)$$

where $\langle \dots \rangle = \int_0^{2\pi} \dots d\theta$ for passing particles

and $\int_A^B \dots d\theta$ for particles trapped between the turning points A and B,

θ being the poloidal angle; S is a source term modelling neutral beam injection. Adopting the coordinate system $v_{\parallel 0} = v_{\parallel}(\theta=0)$,

$v_{10} = v_1(\theta=0)$ and performing the relevant transformations, the r.h.s. of eq. (21) can be written as:

$$\vec{\nabla}_0 \cdot \vec{\Gamma}_{10} + \frac{1}{\langle \frac{v_{110}}{v_{11}} \rangle} \left[\vec{\nabla}_0 \cdot \left(\langle \frac{v_{11}}{v_{110}} \rangle \vec{\Gamma}_{20} + \vec{\Gamma}_{30} \right) + \langle \frac{v_{110}}{v_{11}} S \rangle \right], \quad (22)$$

where the fluxes Γ_{10} , Γ_{20} , Γ_{30} are given by:

$$\vec{\Gamma}_{10} = (\beta/2v_t^2) \left(f + \frac{v_{11}^2}{v^2} (v_{10} \frac{\partial f}{\partial v_{10}} + v_{110} \frac{\partial f}{\partial v_{110}}) \right) \vec{n}_0, \quad (23a)$$

$$\vec{\Gamma}_{20} = (\gamma/4v^2) \left(v_{110} \frac{\partial f}{\partial v_{10}} - v_{10} \frac{\partial f}{\partial v_{110}} \right) (v_{110} \hat{e}_{10} + v_{10} \hat{e}_{110}), \quad (23b)$$

$$\vec{\Gamma}_{30} = \frac{D}{(1+\epsilon)v_{11R}} \left(v_{110} \frac{\partial f}{\partial v_{10}} + \epsilon v_{10} \frac{\partial f}{\partial v_{110}} \right) \left(\hat{e}_{10} + \frac{\epsilon v_{10}}{v_{110}} \hat{e}_{110} \right). \quad (23c)$$

For passing particles:

$$\langle v_{110}/v_{11} \rangle = 4K(1/m), \quad (24)$$

$$\langle v_{11}/v_{110} \rangle = 4E(1/m), \quad (25)$$

where $m = v_{110}/v_{10}(2\epsilon)^{1/2}$, $\epsilon = r/R$; K and E are the elliptic integrals of first and second type respectively.

For trapped particles:

$$\langle v_{110}/v_{11} \rangle = 4mK(m), \quad (26)$$

$$\langle v_{11}/v_{110} \rangle = \frac{4}{m} [E(m) - K(m)(1-m^2)]. \quad (27)$$

The value of v_{\parallel} at resonance, $v_{\parallel R}$, is:

$$v_{\parallel R} = v_{\parallel 0} \left(1 - \frac{1}{2} m^2 \right)^{1/2}. \quad (28)$$

Collecting the expressions (22-28), we see that eq. (21) has also the form of a linear PDE, so that the numerical treatment outlined in section 3 can be straightforwardly applied for its solution.

However, in the situations involving velocity space asymmetry, e.g. current drive, the distribution function must satisfy a further condition. Specifically, it has to be even in $v_{\parallel 0}$ in the trapped particle region [5]. This is normally accomplished by solving the equation in two regions, with the appropriate matching conditions at the boundary. Here, we adopt a "pragmatic" approach which consists in solving the equation in the full domain and after each time step imposing the symmetry

$$f(v_{\parallel 0}, v_{\perp 0}) \rightarrow \frac{1}{2} [f(v_{\parallel 0}, v_{\perp 0}) + f(-v_{\parallel 0}, v_{\perp 0})] \quad (29)$$

in the trapped region. There is a plausible physical argument behind this procedure. In fact, it is equivalent to setting the time step equal to a bounce period. However, since it would be impractical to restrict the time step size to a bounce time, the only criterion adopted is the maximal change of the distribution function.

The results obtained up to now appear physically reasonable, even though the procedure awaits a comparison with other methods in order to be justified.

5. NUMERICAL TESTS

In this section we present some representative results obtained by running BACCHUS in the following conditions:

- 1) No E-field, no waves
- 2) "Small" E-field, no waves
- 3) "Large" E-field, no waves
- 4) "Large" E-field, LH waves

For the ICRF version of BACCHUS, a power deposition test is presented.

5.1 E = 0, D_{RF} = 0

In this case, since no source of energy is present the initial distribution function (Maxwellian) should not evolve under the action of the collision operator. However, the discretization procedure is equivalent to introducing of a source term in the r.h.s. of eq. (1a), so that the system undergoes a "numerically induced" evolution. As a global measure of the discretization error we take the deviations of the parallel and perpendicular kinetic energies from their initial values:

$$\begin{aligned} \delta K_x^0 &\equiv K_x(t=0) - \frac{1}{2} \quad , \quad \delta K_y^0 \equiv K_y(t=0) - 1 \quad , \\ \delta K_x^\infty &\equiv K_x(t \gg \tau_c) - \frac{1}{2} \quad , \quad \delta K_y^\infty \equiv K_y(t \gg \tau_c) - 1 \quad , \end{aligned}$$

where τ_C is the bulk collision time.

In Fig. 3 we show δK_x^0 , δK_y^0 for a uniform (curves 1,2) and non-uniform (curves 3,4) mesh, with boundary at $-10,+10$ for v_{\parallel} and $0,10$ for v_{\perp} . In Fig. 4 the quantities, δK_x^{∞} , δK_y^{∞} , are shown. The quantity h^2 in abscissa is defined as $1/(N_x-1)(N_y-1)$. From Fig. 3 we observe a uniform h^2 convergency law which stems from the fact that the way how the inner products are performed

$$\langle g, f \rangle = \sum_{i=1}^N \sum_{j=1}^N g_i A_{ij} f_j \quad (30)$$

is equivalent to the trapezoidal rule. The real approximation error associated to the numerical treatment is shown in Fig. 4. From this figure we see that to achieve the h^2 error decay rate, something like 1000 nodes are needed, which, for the present case, corresponds to a mesh cell size of about 0.4 in both directions. Moreover, the convergency is from below in agreement with conventional theory. Finally, we remark the beneficial effect of the mesh accumulation technique (at $|v_{\parallel}|=v_{\perp}=1.5$ in the present case), which is particularly apparent for δK_y .

5.2 $E \ll E_D$, $D_{RF} = 0$

When a steady electric field is present, eq. (1) does not admit a steady-state solution. This is due to the runaway electrons ($v > v_C$) which, after a time $\tau_R \sim v_{ee}^{-1} \cdot v_C^3$, go into a free-acceleration regime in which the collisional drag is no longer able to balance the action of the electric field. This means that, unless some further

physical mechanisms are included, the whole electron population will move into the runaway regime in which the current linearly increases in time without limit.

However, if the electric field is sufficiently small, $E \ll E_D$, the runaway time scale, τ_R , is so large that for times of practical interest the system can reach a quasi-steady state. In these conditions, the current will saturate at a value proportional to the strength of the electric field, the constant of proportionality being the Spitzer-Härm conductivity. In Figure 5 we show the values of j/E for the following cases. Curves 1 and 2 refer to a standard non-uniform mesh with boundary at 10 and 16, respectively, curve 3 to a uniform mesh with boundary at 10; in all cases $E = 0.05$. The label SH refers to the Spitzer-Härm value. We see that all three curves converge to a value ~ 1.4 which is roughly 0.7 of the value given by Spitzer-Härm (1.96). This is not surprising since our collision operator has been modified for $v \sim v_{te}$ and therefore it is not expected to yield a particularly accurate description of the phenomena which occur in the thermal region. Thus, this test can be regarded as positive.

From Fig. 5 we notice the benefit arising from the mesh accumulation technique. Even with a 20×10 grid we have $j = 1.385 \times 10^{-2}$, compared with the value $j = 1.414 \times 10^{-2}$ obtained with the 80×40 grid. This implies that the mesh accumulation technique yields reasonable results even with very coarse grids. This property will be better appreciated from the results of the next test.

5.3 $E < E_D, D_{RF} = 0$

When the electric field becomes larger than some percent of the Dreicer field the runaway phenomenon becomes dominant. The main physical quantity of interest is the runaway rate, A , defined as the fraction of the electrons which run away from the bulk population per unit of time: $A = |\dot{n}/n|$, n being the electron density. The equation for the density evolution in the domain Δ reads

$$\dot{n} = E F(v_{||} = V_2) \quad , \quad (31)$$

where $F(v_{||}) = \int_0^{V_2} f(v_{||}, v_{\perp}) v_{\perp} dv_{\perp} \quad .$

From eq. (31) we see that to achieve a steady state, $\dot{n} = 0$, a source of particles has to be provided in the r.h.s. of eq. (1a). In BACCHUS such a source is modelled by the following procedure. At each time step the density change δn is computed and the density is renormalized to unity by adding a Maxwellian distribution of particles of density δn . The runaway rate can then be computed either as

$$A = A_n \equiv |\dot{n}/n| \quad , \quad (32.a)$$

or as
$$A = A_F \equiv |E| F(V_2) \quad . \quad (32.b)$$

These expressions imply that we need a high level of accuracy because the detailed shape of the distribution function $F(v_{||})$ is essential.

In Figure 6 we show a test case with $E = 8\%$ and the mesh boundaries at 16; the curve 1 refers to a uniform mesh while for curve 1 a s.n.u. mesh was used. The label K refers to the value given by Kulsrud et al. [6]. Both curves converge approximately to $A=5 \times 10^{-4}$ which is somewhat higher than the value given by Kulsrud et al. $A_K = 3.177 \times 10^{-4}$. (This discrepancy is acceptable if we consider that A_K was obtained with a 75×22 uniform $v - \theta$ mesh). Once again we remark the important role played by the mesh accumulation technique. For the 40×20 non-uniform mesh we have $A_n = 3.88 \times 10^{-4}$ whereas with the same number of uniformly spaced nodes the value of A_n is even not positive ($A_n \sim -1 \times 10^{-5}$)!. As a consequence, in order to get reasonable results with a uniform mesh one needs at least 2000 points, which already overcome the storage capabilities of our CDC-8005 machine if the Gauss elimination method is adopted. This limitation disappears on a CRAY-1 machine where grids up to 5000 points can be used. Incidentally, we remark that on the CRAY the c.p.u. time is reduced by about a factor 7. A typical run on a 40×20 mesh takes about 180 sec on the CYBER-8005 and 25 on the CRAY-1.

Another possibility is to resort to the iterative method described in section 3.4. The performances of this method are summarized in Fig. 7, where we plot the ratio of the runaway rates obtained using the iterative and Gauss methods, A_G/A_I (curve 1), and the corresponding ratio, t_G/t_I , of the c.p.u. times (curve 2). The quantity ϵ_C in abscissa represents the closure value for the iteration cycle. A 40×20 non-uniform mesh is used and no relaxation is adopted. From this figure we see that the iterative procedure is cheaper for

$\epsilon_C < 10^{-3}$, which is unfortunately not sufficient to achieve the correct value of A . This is quite logical since $A_G = 3.88 \times 10^{-4} < 10^{-3}$! Thus, to obtain a reasonable value of A_I we need to push ϵ_C below 10^{-4} , which costs about 10 iterations per time step, resulting in a c.p.u. time considerably higher than that for the Gauss method.

Even resorting to an over-relaxation technique does not lead to any significant progress; this is probably related to a bad condition of the matrix A caused by the advective term (this point should deserve more theoretical investigation). However, if one is interested in global quantities, like the current, then values of $\epsilon_C > 10^{-3}$ can be safely adopted and the iterative procedure proves more convenient also from the point of view of the c.p.u. costs, as the following table shows:

ϵ_C	U_x	U_y	$2K_x$	$2K_y$	$10^4 xA$	$10^2 x t_{CPU}$	$10^3 x t_{EL}$
0.	.6675	1.475	5.470	3.577	3.88	2.65	2.28
0.5	.6704	1.473	5.502	3.586	-6.82	1.02	.445
0.05	.668	1.472	5.471	3.577	.45	1.33	1.02
0.005	.668	1.472	5.471	3.576	.35	1.73	2.23

In this table $U_{x,y}$ are the linear moments, t_{CPU} and t_{EL} are the c.p.u. time and elapsed time respectively. The first line corresponds to the values obtained by the Gauss method. Thus, it seems that an optimal strategy would consist in adopting the iterative method with a low value of ϵ_C until a steady state for the moments is obtained, and subsequently switching to the Gauss method to recover the correct value of A .

5.4 $E < E_D, D_{RF} \neq 0$

It has been shown [7] that the presence of a source of rf waves can greatly enhance the runaway rates. Here, we present a convergency study referring to the following case :

$$|E| = 8\% ,$$

$$D_{LH} = \begin{cases} 600 & , \quad 2 = v_1 \leq v_{||} \leq v_2 = 4 \\ 0 & , \quad \text{otherwise} \end{cases} .$$

The results are reported in Fig. 8, where curve 1 refers to a uniform mesh, curve 2 to a s.n.u. mesh and curve 3 to the same mesh as for 2 but $D_{LH} = 0$. We see that for both the uniform and non-uniform meshes no convergency law can be inferred but rather a fluctuation around an average value of about 3×10^{-3} (roughly 10 times higher than the corresponding value without rf waves) is observed.

This behaviour stems from the poor discretization of the discontinuity in the definition of $D_{LH}(v_{||})$. In particular, the results are sensitive to the locations v_L, v_R of the boundaries of the mesh cell containing v_1 ($v_L < v_1 < v_R$) through a "jittering factor" F_g given approximately by:

$$F_g = \exp(-v_1^2/2) / \exp - \left[\frac{v_L^2}{2} + \int_{v_L}^{v_R} \frac{v \, dv}{1 + D_{LH}(v-v_L)/(v_R-v_L)} \right] .$$

This factor represents the ratio of the plateau heights of the distribution function for a constant D starting exactly from v_1 and for a D linearly increasing from v_L to v_R and constant beyond v_R ,

respectively. Once this correcting factor is taken into account, the scatter in the results for the uniform mesh is practically eliminated. For the non-uniform mesh, however, this is not the case, indicating that the upper boundary of the spectrum, v_2 , also plays a role. In general, all the three points v_1 , v_2 , v_c require a special care in order to obtain a good accuracy. However, since the amplitude of the fluctuations around the average value is rather small, no optimization of the mesh accumulation technique has been performed.

5.5 Power Deposition Test

In a steady state all the power deposited by the waves is dissipated by the collisions, so that the relation

$$\int \frac{v^2}{2} \left(\frac{\delta f}{\delta t} \right)_Q d_3 v = \int \frac{v^2}{2} \left(\frac{\delta f}{\delta t} \right)_{\text{coll}} d_3 v \quad (33)$$

must hold. In the limit of small Larmor radius, $k_{\perp} v_{\perp} / \omega_c \ll 1$, the integral on l.h.s. of eq. (33) can be performed exactly, so that an analytical check on $(\delta f / \delta t)_{\text{coll}}$ is available. The result is shown in Fig. (9), where P_Q and P_c denote the l.h.s. and r.h.s. of eq. (33) respectively. A 40x40 mesh with boundary at -10,+10 in v_{\parallel} and 0,10 (curve 1) and 0,20 (curve 2) in v_{\perp} is used.

From this figure we see that a good agreement is achieved up to a given value, P_{QM} , of P_Q after which a significant deviation is observed in curve 1. This is to be interpreted as a finite-boundary effect. In fact, for $P_Q > P_{QM}$ the distribution function is distorted and dragged far out, so that to recover a good agreement an extension of the boundary (curve 2) in v_{\perp} is needed.

6. RUNAWAY; A 1 1/2-D QUASI-LINEAR CODE

In this section we shall discuss the main features of the 1 1/2-D quasi-linear code RUNAWAY. We shall not present an extensive numerical study but rather illustrate the basic difficulties inherent to the self-consistent treatment of the wave-particle interaction.

6.1 The Physical Model

RUNAWAY is devised to solve the evolution equation for the electron distribution function:

$$\left(\frac{\partial f}{\partial t}\right) = \left(\frac{\delta f}{\delta t}\right)_{\text{COLL}} + \left(\frac{\delta f}{\delta t}\right)_{\text{IND-E}} + \left(\frac{\delta f}{\delta t}\right)_{\text{QL}} \quad (34)$$

and for the simultaneous evolution of the wave spectral distribution $W(k,t)$:

$$\frac{\partial W}{\partial t} = \Gamma W + S \quad (35)$$

with the initial conditions $f(\vec{v},0)=\phi(\vec{v})$ and $W(\vec{k},0)=W_0$, where S is an external source and ϕ is an arbitrary function which can also model unstable situations [8]. The normalizations adopted are: $k \rightarrow k/\lambda_D$, $t \rightarrow t/\omega_{pe}$, $W \rightarrow W \cdot 4\pi n T \lambda_D^3$, $E \rightarrow E (4\pi n T \lambda_D^3)^{1/2}$, where λ_D is the electron Debye length. The terms $(\delta f/\delta t)_{\text{COLL}}$ and $(\delta f/\delta t)_{\text{IND-E}}$ have the same meaning as in BACCHUS, with an additional option for $(\delta f/\delta t)_{\text{COLL}}$ which can be either the 2-D collision operator already described in section 1, or its simplified 1-D version (Vedenov):

$$(2+Z) \nu_{ee} \frac{\partial}{\partial v_{\parallel}} \left[n_{\parallel}^{-3} (n_{\parallel} f + \frac{\partial f}{\partial v_{\parallel}}) \right] .$$

The essential difference with respect to BACCHUS consists of the presence of the term $(\delta f / \delta t)_{QL}$ which describes the resonant diffusion processes due to the Cerenkov ($l=0$) and the first anomalous Doppler ($l=1$) resonances:

$$\left(\frac{\delta f}{\delta t}\right)_{QL} = \sum_{l=0}^1 \left(\frac{\partial}{\partial v_{\parallel}} - \frac{l v_{\parallel}}{v_{\perp}}\right) D_l \left(\frac{\partial}{\partial v_{\parallel}} - \frac{l v_{\parallel}}{v_{\perp}}\right) f \quad (36)$$

with

$$D_l = \left(\frac{\pi}{2^{2l-1}}\right) \int_{k_{\parallel} > 0} \frac{d^3 k}{(2\pi)^3} \left(\frac{k_{\parallel}}{k_{\perp}}\right)^2 \left(\frac{k_{\perp} v_{\perp}}{\omega_{ce}}\right)^2 \delta(\omega_{k\ell} - k_{\parallel} v_{\parallel}) W(\vec{k}, t)$$

and $\omega_{k\ell} = \ell \omega_{ce} + k_{\parallel} / k$, ω_{ce} being the electron cyclotron frequency.

In these expressions the dispersion relation $\omega_k = k_{\parallel} / k \ll \omega_{ce}$ was assumed for the magnetized Langmuir waves, so that one has $\omega_{k0} = k_{\parallel} / k$ and $\omega_{k1} = \omega_{ce}$.

The factor Γ in the r.h.s. of eq. (35) represents the total, collisional and resonant, wave damping given by:

$$\Gamma = 2 (\gamma_0 + \gamma_1 - \gamma_{ee} Z/4) \quad (37)$$

with

$$\gamma_l = \left(\frac{\pi}{2^{2l+1}}\right) \frac{k_{\parallel}^2}{k^3} \int d^3 v \left(\frac{k_{\perp} v_{\perp}}{\omega_c}\right)^{2l} \left(\frac{\partial}{\partial v_{\parallel}} - \frac{l v_{\parallel}}{v_{\perp}} \frac{\partial}{\partial v_{\perp}}\right) f \delta(\omega_{k\ell} - k_{\parallel} v_{\parallel}) .$$

Equations (34-35) describe a rich variety of physical phenomena which have been treated quite extensively in the literature. A discussion of these phenomena is beyond the scope of the present paper. For the present purposes it is sufficient to note that eqs. (34-35) are two coupled integro-differential equations which have to be solved in

the two-dimensional spaces $D_v \equiv \{v_{\parallel}, v_{\perp} ; -\infty < v_{\parallel} < +\infty, v_{\perp} \geq 0\}$ and $D_k \equiv \{k_{\parallel}, k_{\perp} ; k_{\parallel} > 0, k_{\perp} \geq 0\}$.

7. THE NUMERICAL TREATMENT

7.1 Discretization of the Electron Distribution Function

In order to solve eq. (34) a special semi-discrete finite-element method has been adopted. More specifically, a solution is sought in the form:

$$f(v_{\parallel}, v_{\perp}, t) = \sum_{j=1}^N f_j(t) \Psi_j(v_{\parallel}) \left(2\pi T_j(t)\right)^{-1} \exp\left(-v_{\perp}^2/2T_j(t)\right), \quad (38)$$

where Ψ_j are the usual roof functions. The set of discrete parallel velocities $\{v_{\parallel j}; j=1, N_x\}$ covers a finite interval $J=\{v_{\parallel}; V_1 < v_{\parallel} < V_2\}$. A non-equidistant mesh is allowed. The reason for such a choice is the fact that the selection rules represented by the Dirac distributions only involve the parallel velocities. Thus, one can reasonably assume the evolution in the perpendicular direction to be self-similar, and consequently treat it by a set of global functions of pre-assumed Maxwellian shape.

The advantage of this method is that the 2-D problem is reduced to a 1-D problem for the $2 \cdot N_x$ unknowns $f_j, g_j; j=1, N_x$. Apart from the limitation on the class of functions representable by the ansatz (38), there are also disadvantages from the computational point

of view. In fact, the equations governing the evolution of $f_j(t)$, $T_j(t)$ will inherit the non-linearity of the ansatz (38) with respect to T_j . Whether or not this bargain is profitable depends on the degree of complexity of the operators acting in the perpendicular direction, as we shall discuss more in detail later on.

The ansatz (38) is substituted into eq. (34) which is in turn projected onto the two sets of basis functions $\Psi_j(v_{\parallel})$ and $1/2v_{\perp}^2 \Psi_j(v_{\parallel})$ to obtain the following set of O.D.E.:

$$\sum_{j=1}^N A_{ij} \dot{f}_j = \sum_{j=1}^N (B_{ij}^0 + B_{ij}^1) f_j, \quad (39)$$

$$\sum_{j=1}^N A_{ij} \dot{g}_j = \sum_{j=1}^N (B_{ij}^0 + C_{ij}^1) g_j, \quad (40)$$

where $g_j = f_j T_j$. The explicit expressions for the matrices A, B, C are given in Ref. [8]; here we only mention that superscript 1 labels the matrices which are affected by the non-linearity discussed above. More specifically, they are the matrices representing the anomalous Doppler and 2-D Fokker-Planck operators.

7.2 Discretization of the Wave Spectral Distribution

The discretization of the wave spectrum is performed using a 2-D finite element expansion:

$$W(k_{\parallel}, k_{\perp}, t) = \sum_{k=1}^M W_k(t) \chi_k(k_{\parallel}, k_{\perp}). \quad (41)$$

Since the wave equation (35) is algebraic with respect to \vec{k} , the basis functions $\chi_k(\vec{k})$ are chosen to be piecewise constants on rectangular supports of irregular size, covering a finite domain Δ_k in the plane $(k_{\parallel}, k_{\perp})$. The domain Δ_k is constructed on the basis of the discrete sequence $\{v_{\parallel j}\}$ in such a way as to guarantee a high density of Cerenkov and Doppler interaction lines: $k=1/v_{\parallel}$ and $k_{\parallel}=\omega_{ce}/v_{\parallel}$ [3].

The set of basis functions, $\{\chi_k\}$, is orthogonal so that by projecting eq. (35) onto it we obtain the following diagonal system of O.D.E.

$$\dot{W}_k = \Gamma_k W_k + S_k \quad (42)$$

for the M unknowns W_k , $k=1, M$.

7.3 Time Discretization

Eqs. (39), (40) and (42) are integrated with a synchronous 2-level scheme. In matrix notation:

$$A \cdot \left(\frac{f_{n+1} - f_n}{\Delta t} \right) = \left(B^{(0)} + B^{(1)}(W_{n+1/2}, T_{n+1/2}) \right) \cdot f_{n+1/2} \quad (43a)$$

$$A \cdot \left(\frac{g_{n+1} - g_n}{\Delta t} \right) = \left(B^{(0)} + C^{(1)}(W_{n+1/2}, T_{n+1/2}) \right) \cdot g_{n+1/2} \quad (43b)$$

$$W_{n+1} = \exp(\Gamma_{n+1/2} \Delta t) \cdot W_n + \left(\frac{\exp(\Gamma_{n+1/2} \Delta t) - 1}{\Gamma_{n+1/2}} \right) S_n \quad (43c)$$

$$\Gamma_{n+1/2} \equiv \Gamma_{n+1/2} (f_{n+1/2}, g_{n+1/2}), \quad \Delta t \equiv t_{n+1} - t_n,$$

where the time level $n+1/2$ is defined by the interpolation

$$f_{n+1/2} = f_{n+1} \delta + f_n (1-\delta)$$

with $0 < \delta < 1$.

This scheme, which is solved by an iterative technique, has the advantage to ensure unconditional stability and second order accuracy (if $\delta=1/2$) with a fairly moderate requirement on algebraic complexity. In fact, since all the matrices have a simple 3-diagonal structure, they can be treated by very fast algebraic solvers.

However, owing to the self-consistent treatment of the wave-particle interaction, the numerical scheme must be able to handle also truly, i.e. physically, unstable situations. This implies that the automatic time-step control system must become more severe. For this reason, in addition to the usual control of the maximum relative changes of f, g, W a further constraint is imposed on the time step Δt :

$$\Gamma_{\max} \Delta t < c, \quad (44)$$

where c is the maximum change allowed and $\Gamma_{\max} = \text{Max}_k \{\Gamma_k\}$. We would like to pinpoint how delicate this control is: if some wave is excited by a purely numerical accident (typically a ripple at high v_{\parallel} produced by electric field convection), the time evolution can be drastically slowed down without any physically acceptable reason.

Nevertheless, apart from any numerical trouble, the system possesses several time scales in different regions of the velocity space, so that a fair amount of stiffness has to be expected.

7.4 Method of Solution

The system of O.D.E. (43) is non-linear and must therefore be solved by an approximation technique. We adopt Picard's successive iteration method which leads to the following cycle:

$$A_f^{(\ell)} \cdot f_{n+1}^{(\ell+1)} = B_{f, n+1/2}^{(\ell)} \cdot f_n \quad , \quad (45a)$$

$$A_g^{(\ell)} \cdot g_{n+1}^{(\ell+1)} = B_{g, n+1/2}^{(\ell)} \cdot g_n \quad , \quad (45b)$$

$$W_{n+1}^{(\ell+1)} = B_{w, n+1/2}^{(\ell)} \cdot W_n + S_{n+1/2}^{(\ell)} \quad , \quad (45c)$$

where the meaning of the symbols follows directly from eqs. (43).

As usual, the cycle is closed whenever the maximal deviation, $\varepsilon(\underline{X}^{l+1}, \underline{X}^l)$, of the unknown array $\underline{X} \equiv \{f, g, W\}$ between two successive iterations falls below a given threshold ε_C . If this is not the case after ten iterations the time integration continues, but the next time step is reduced. At this point we could exhibit a series of tests which would illustrate the convergency properties of RUNAWAY in some simple cases like those described in section 5. However, since RUNAWAY was devised for studying more complex physical phenomena, we find it more instructive to pass directly to the discussion of the basic problems encountered when dealing with such phenomena.

8. TYPICAL NUMERICAL PROBLEMS

In this section we give a brief qualitative account of the performances of RUNAWAY in various physical conditions. No rigorous argument is brought, but rather the conclusions drawn from the experience of running the code. The main question on RUNAWAY efficiency concerns the convergence of the iterative scheme, eqs. (45). We shall therefore examine how the various unconventional features included in RUNAWAY can affect such a scheme.

8.1 The Role of the Wave-Particle Interactions

As long as only the Cerenkov resonance is included, no serious problem has ever been met: the code is reliable and a steady state is rapidly achieved. This is comprehensible since the Cerenkov interaction is represented by a diffusion matrix which is proportional to the wave amplitude, W . It means that $-B_{ij}^{(Cer)}$ is positive definite provided $W > 0$, a condition which is always guaranteed since W is not allowed to decrease below a minimum threshold, W_{noise} . Moreover, since a good resolution is achievable (we can put more than 100 nodes along $v_{||}$), no ripples are generated on the distribution function and no artificial instability is triggered.

Once the anomalous Doppler interaction is included, the situation becomes a little more complicated because additional physically unstable situations can arise in conjunction with the presence of a steady electric field. Moreover, the corresponding matrices are

affected by the non-linearity stemming from the ansatz (38).

Particularly critical situations can arise during the development of the Parail-Pogutse instability [9]. More specifically, overshoots can appear on the tip of the unstable distribution function when the anomalous Doppler effect is acting against E-field to push back the runaway electrons. This problem is partially solved by chopping dynamically the mesh in such a way as to exclude the "ill" portion of the distribution function. The careful resort to these expedients is usually successful, but the operation of the code requires a sort of assistance which is hardly acceptable in a long-period exploitation.

8.2 Role of the Non-Linearity

To get an idea of the role played by the non-linearity introduced by the ansatz (38), let us perform a sort of "stability" analysis of the matrices representing the anomalous Doppler interaction. We can write:

$$B_{ij}^{(1)} = \sum_{l,m=0}^1 \langle \psi_i^{(l)} b_{lm}(\vec{v}, T) \psi_j^{(m)} \rangle ,$$

$$C_{ij}^{(1)} = \sum_{l,m=0}^1 \langle \psi_i^{(l)} c_{lm}(\vec{v}, T) \psi_j^{(m)} \rangle ,$$

where $\psi^{(l)} \equiv d^l \psi / d v_{||}^{(l)}$.

The non-linear terms are $b_{11} \sim -T$, $c_{00} \sim 1/T$ and $c_{11} \sim -T$. Since the numerical approximation of the advective operators in eq. (34) can lead

to negative values of both f and g , eqs. (39) and (40), we must distinguish four cases:

1) $f, g > 0$ ($T > 0$)

This is a physically meaningful region.

2) $f > 0, g < 0$ ($T < 0$)

The terms b_{11} and c_{11} tend to produce negative diffusion, i.e. steepening rather than smoothing of the gradients in the course of time. However, there is also a beneficial effect arising from c_{00} which tends to make g positive hence restoring the "healthy" case 1.

3) $f < 0, g < 0$ ($T > 0$)

In this case no "fake diffusion" occurs, but the term c_{00} tends to make g more and more negative so that the temperature increases. However, due to the $1/T$ dependence of c_{00} , this growth is self-controlled.

4) $f < 0, g > 0$ ($T < 0$)

Repeating the same arguments as for case 2, a transition towards case 3 is expected.

If we imagine the evolution of two local values $f_i(t)$, $g_i(t)$ as a trajectory in a plane f, g , we see that once the representative point $P \equiv (f, g)$ is moved away from the "healthy" region, for example by the steady electric field, its fate becomes in a sense "aleatory" and the code can become very inefficient. In order to avoid this type of problems it is often necessary to set a pedestal on T , $T > T_0 > 0$, in

such a way that the "motion" of the representative point is confined to the regions 1 and 3.

Up to now the "experiment" with the non-linear ansatz (38), can be regarded as successful since, even with some difficulty, the code is able to follow quite complicated physical situations. The reason for this is very likely the fact that the non-linearity introduced into the anomalous Doppler operator is relatively moderate.

For the 2-D collision operator the situation is unfortunately much more critical. The expressions for the coefficients b_{lm} and c_{lm} as functions of T become so complicated that even a qualitative analysis of the type sketched above seems hardly feasible, unless one takes the limit of small deviations of T from the equilibrium value 1. From the empirical point of view, this operator performs well in combination with the Cerenkov operator, starts to pose some problems with the inclusion of the anomalous Doppler operator, and it is very unreliable if the electric field is also included. On the other hand, if we consider recent developments in the lower-hybrid current drive (ramp-up, start-up), it is clear that the inclusion of the electric field is indispensable.

For this reason, after some attempts to improve the code, we have come to the conclusion that the advantages gained from the non-linear ansatz are overbalanced by the numerical problems. As a consequence, we have decided to move in a new direction, as we shall briefly mention in the concluding section.

9. CONCLUSIONS

We have presented two codes, BACCHUS and RUNAWAY, for the numerical investigation of a certain class of wave-particle interactions.

BACCHUS can be regarded as a general and reliable 2-D Fokker-Planck solver with a flexible structure. It has been used to compute the enhancement of the runaway rates in the presence of a source of LH or/and EC waves [10]. More recently, the ICRF version has been used to investigate problems of particle trapping in ICRF-BEAM heated tokamak plasmas [11]. This type of studies, together with investigations on minority ion current drive by ICRF heating are presently being carried out at JET.

RUNAWAY deals with a much more complex physics, but its structure is to a large extent tied to an assumption on the shape of the electron distribution function which is suggested by physics itself. Its performance is not uniform, but deteriorates with the increasing complexity of the weak turbulence processes that need to be described. The possibility of replacing the ansatz (38) with a more conventional expansion in a series of classical polynomials was investigated. The result of this analysis indicates that, for situations far from equilibrium, it is impossible to obtain everywhere positive solutions without resorting to an unacceptably high number of polynomials. For this reason, we finally decided to adopt a 2-D finite element method, in which both the electron and the wave spectral distributions are expanded in a series of two-dimensional local basis functions. A quasi-linear code based on this method has been written, and is presently in a very preliminary testing stage at CRPP.

REFERENCES

- [1] M.G. McCoy, G.D. Kerbel and R.W. Harvey, contributed paper presented at this Conference
- [2] G. Strang and G.J. Fix, "An Analysis of the Finite Element Method" (Prentice-Hall, Englewood Cliffs, 1973)
- [3] K. Appert, T.M. Tran and J. Vaclavik, Comp. Phys. Commun. 12 (1976) 135
- [4] K.V. Roberts, Comp. Phys. Comm. 7 (1974) 237
- [5] J.G. Cordey, Nucl. Fusion 16 (1976) 499
- [6] R.M. Kulsrud, Y.-C. Sun, N.K. Winsor and H.A. Fallon, Phys. Rev. Lett. 31 (1973) 690
- [7] C.S. Liu, Z.G. An, D.A. Boyd, Y.C. Lee, L. Muschietti, K. Appert and J. Vaclavik, Comments Plasma Phys. Contr. Fusion 7 (1982) 21
- [8] L. Muschietti, K. Appert and J. Vaclavik, Phys. Fluids 24 (1981) 151
- [9] V.V. Parail and O.P. Pogutse, Sov. J. Plasma Phys. 2 (1976) 125
- [10] K. Appert, A.H. Kritz, S. Succi and J. Vaclavik, Proc. of 11th EPS Conf. on Contr. Fus. Plasma Phys., Aachen (1983), Paper B29
- [11] T. Hellsten, K. Appert, W. Core, H. Hamnén and S. Succi, to be published in the Proc. of 12th EPS Conf. on Contr. Fus. Plasma Phys., Budapest (1985)

FIGURE CAPTIONS

- Fig. 1 Bilinear basis function.
- Fig. 2 The numbering of nodal points.
- Fig. 3 The deviations of the parallel (1,3) and perpendicular (2,4) kinetic energies at $t=0$ from the exact values versus h^2 . Curves 1, 2 and 3, 4 refer to uniform and non-uniform meshes, respectively.
- Fig. 4 The deviations of the parallel (1,3) and perpendicular (2,4) kinetic energies at $t=\infty$ from the exact values versus h^2 . Curves 1, 2 and 3, 4 refer to uniform and non-uniform meshes, respectively.
- Fig. 5 Dimensionless conductivity versus h^2 . Curves 1 and 2 refer to a non-uniform mesh with boundary at 10 and 16 respectively, curve 3 to a uniform mesh with boundary at 10. The dot-and-dashed line refers to the Spitzer-Härm value.
- Fig. 6 Runaway rate versus h^2 . Curves 1 and 2 refer to uniform and non-uniform meshes.
- Fig. 7 Ratio of the runaway rates obtained using the iterative and Gauss method (1) and the corresponding ratio of the c.p.u. times (2). The quantity ϵ_c represents the closure value for the iteration cycle.
- Fig. 8 Enhanced runaway rate versus h^2 . Curves 1 and 2, 3 refer to uniform and non-uniform meshes, respectively.
- Fig. 9 Power dissipated by collisions P_c versus power deposited by waves P_Q . A 40x40 mesh with boundary at $|v_{\parallel}| = 10$ and $v_{\perp} = 10$ (curve 1), and $v_{\perp} = 20$ (curve 2) is used.

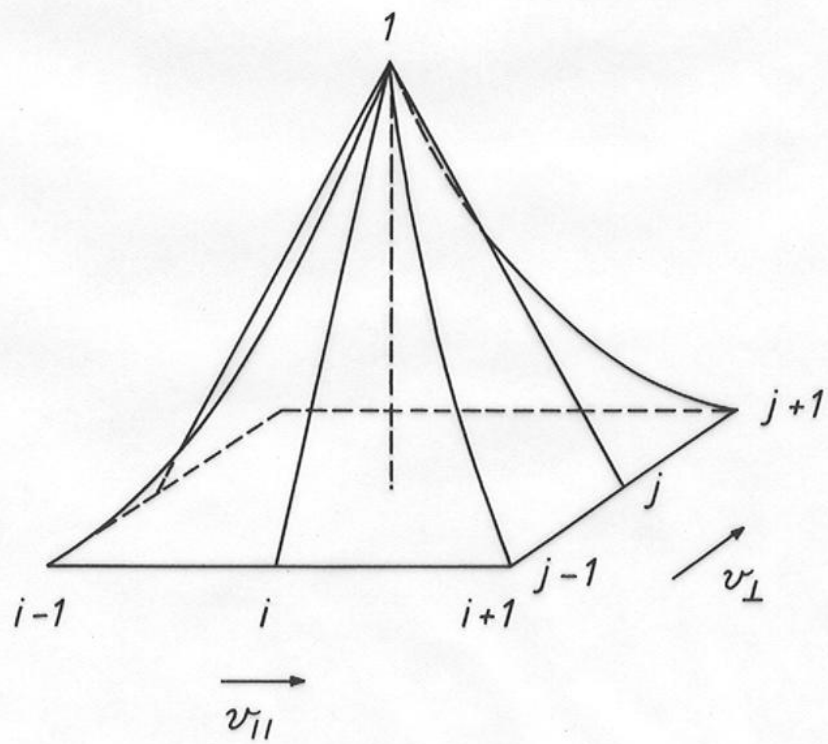


FIG. 1

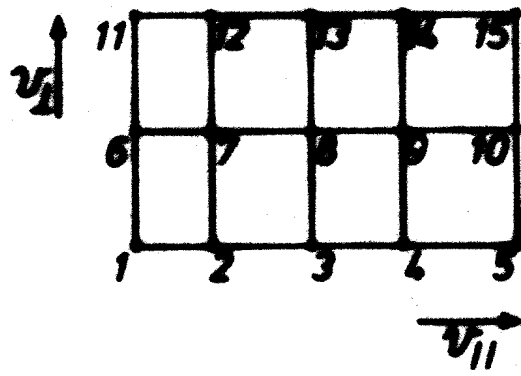


FIG. 2

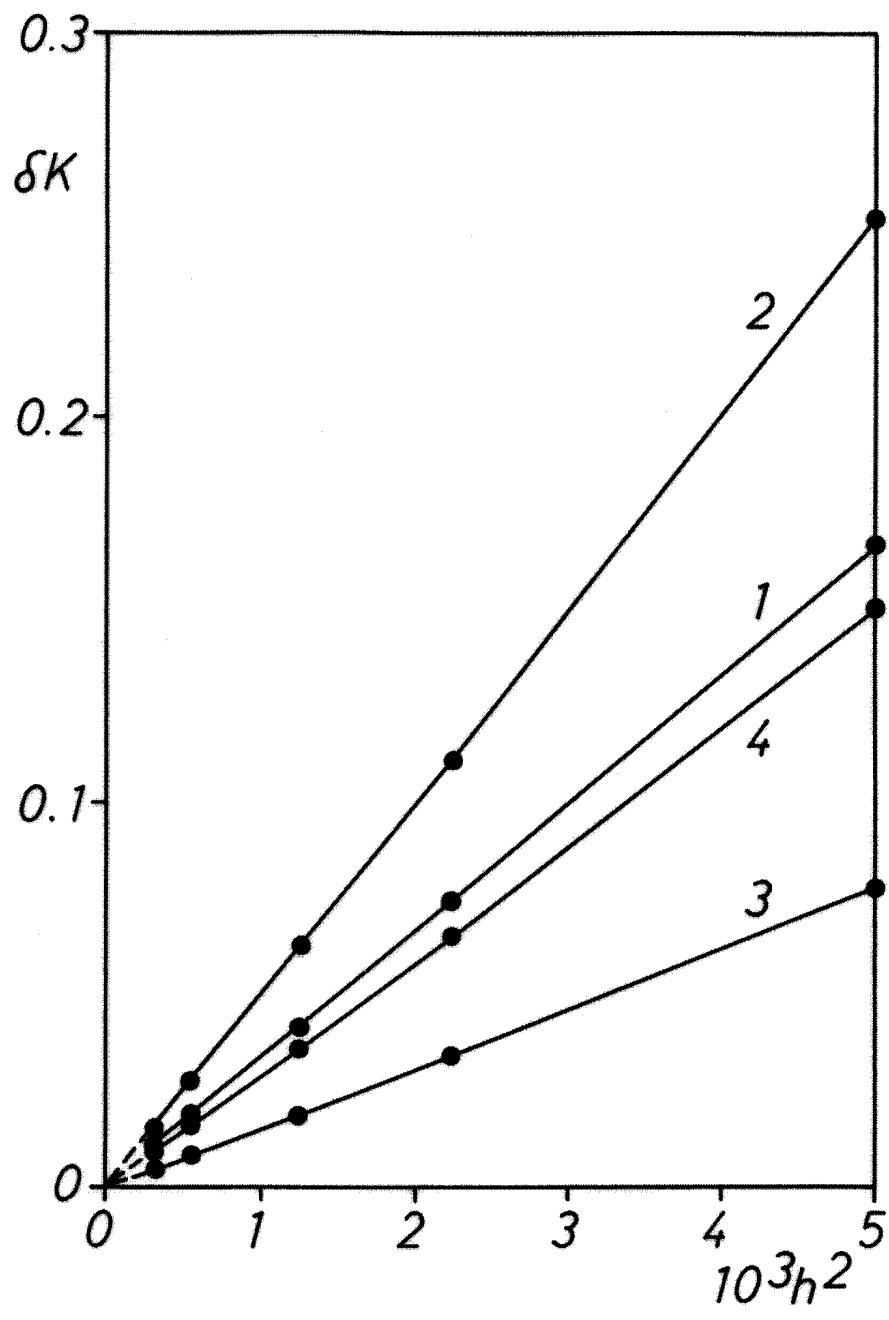


FIG. 3

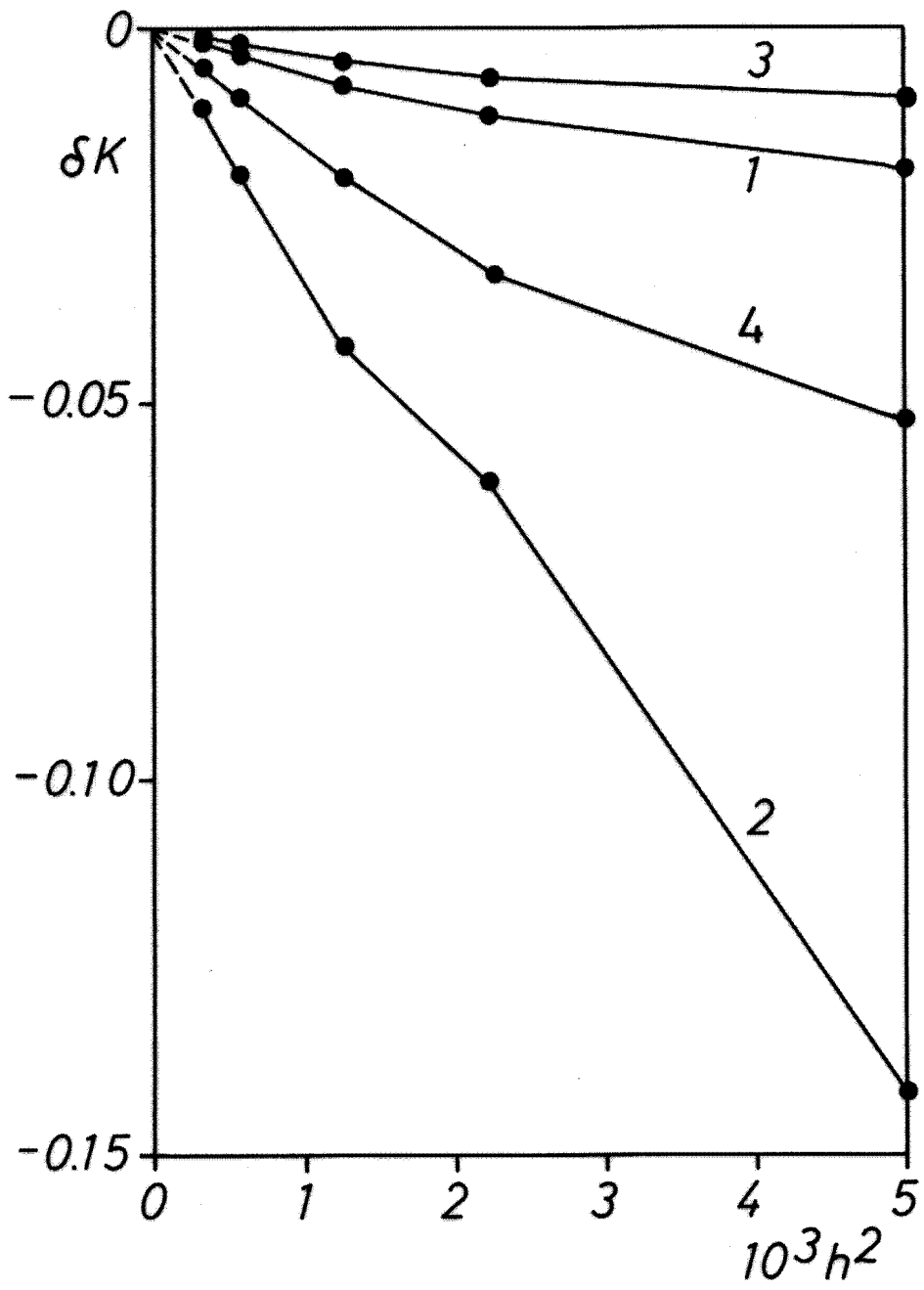


FIG. 4

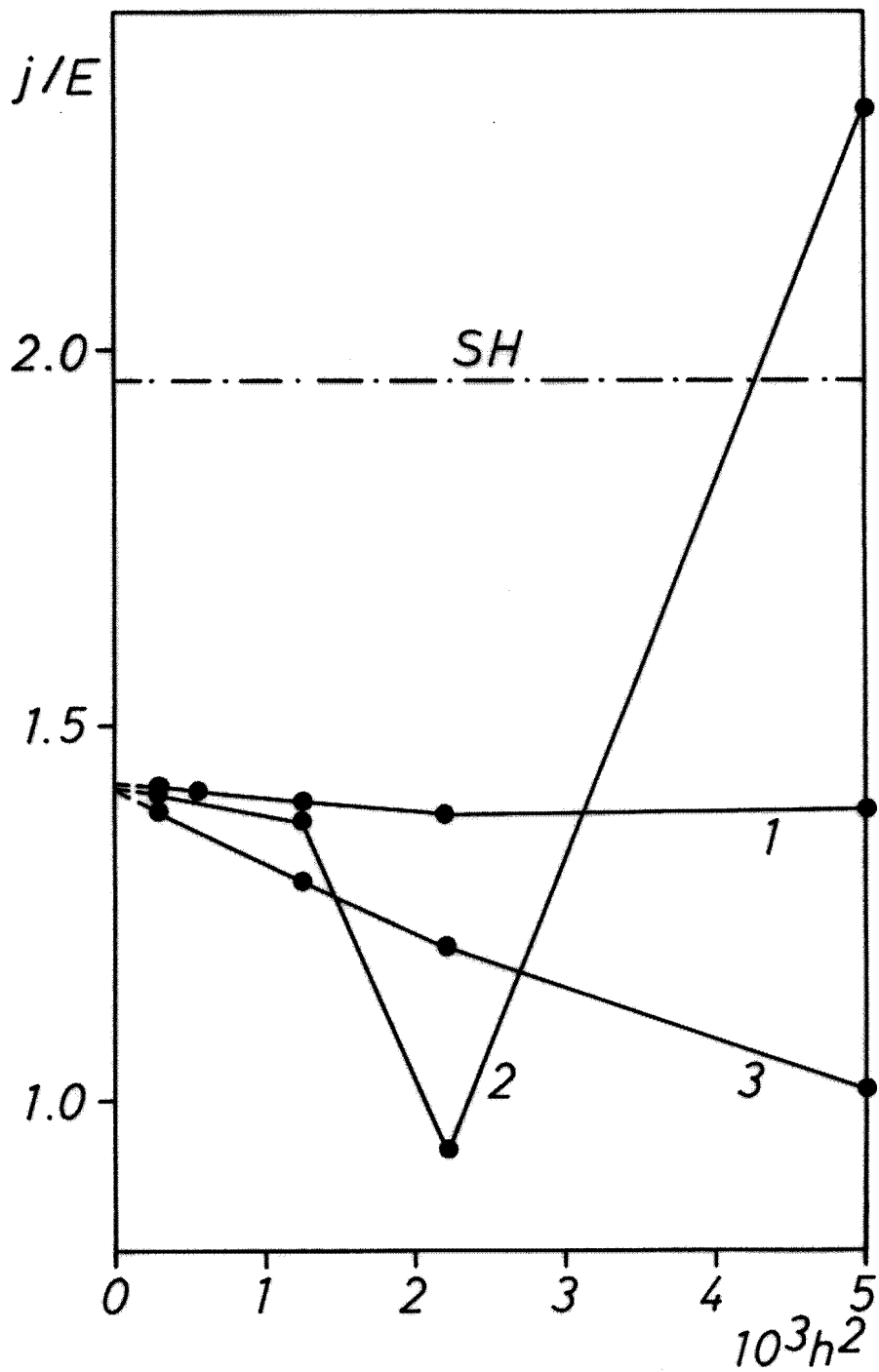


FIG. 5

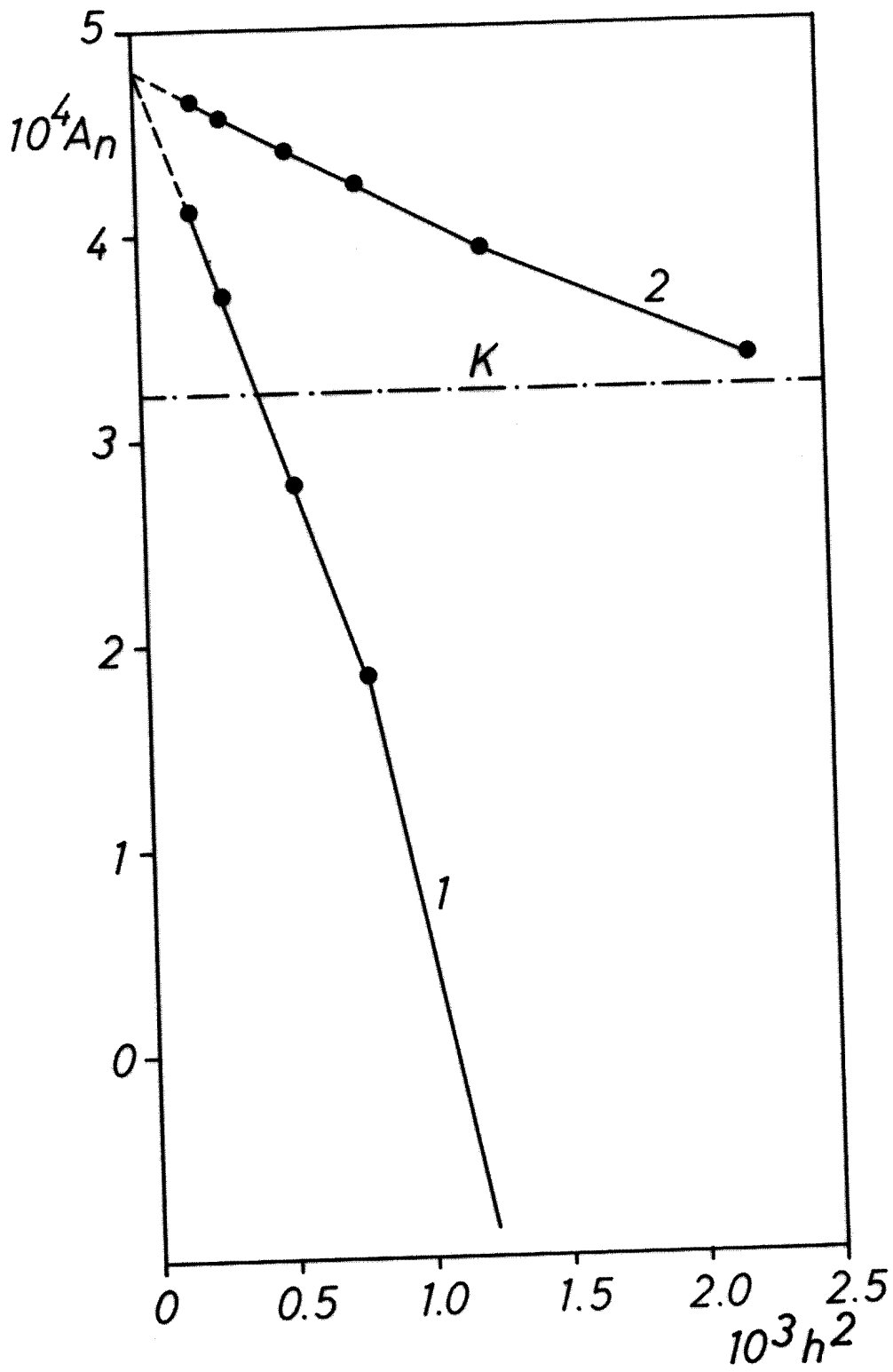


FIG. 6

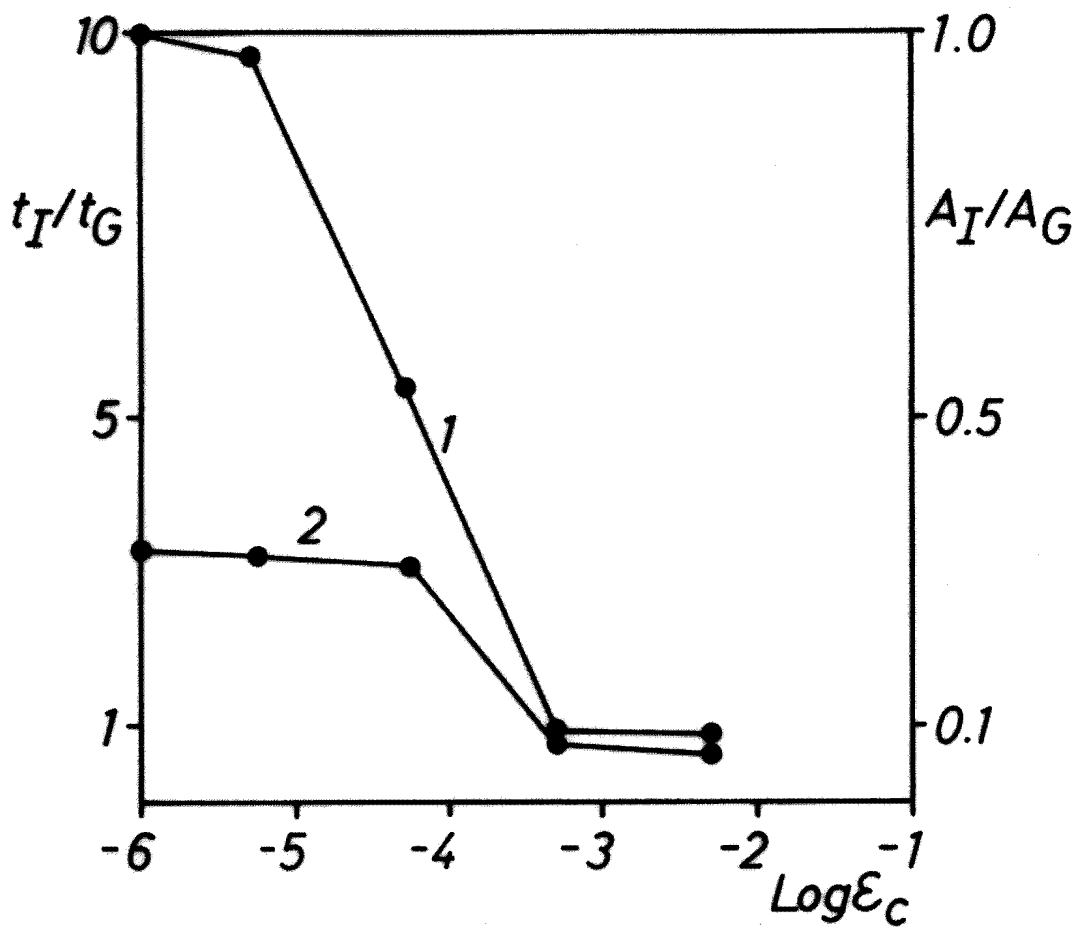


FIG. 7

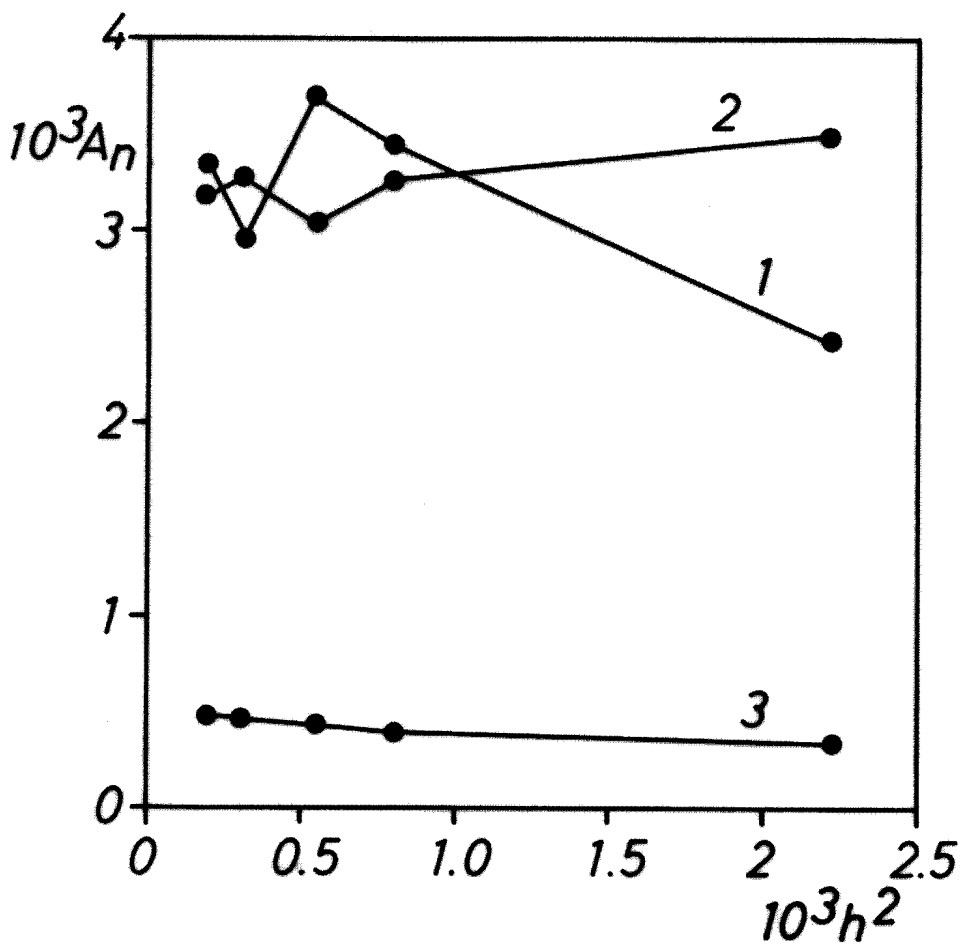


FIG. 8

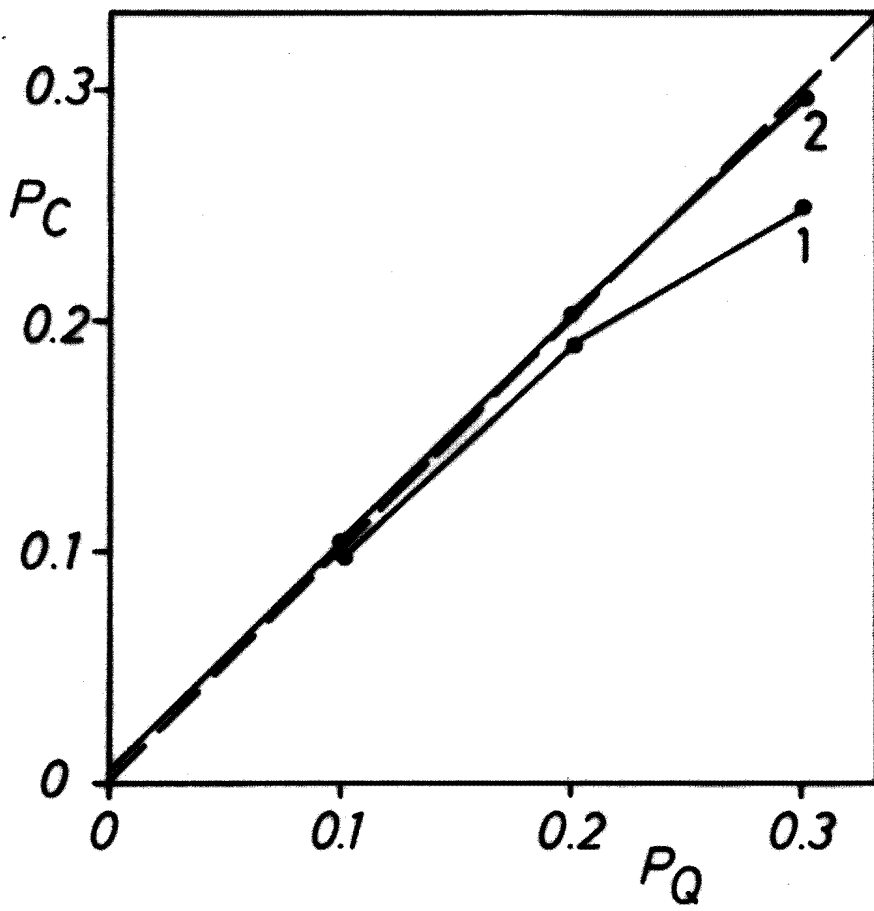


FIG. 9